Permanently hydrophilic, piezoelectric PVDF nanofibrous scaffolds promoting unaided electromechanical stimulation on osteoblasts

Maria Kitsara, Andreu Blanquer, Gonzalo Murillo, Vincent Humblot, Sara de Bragança Vieira, Carme Nogués, Elena Ibáñez, Jaume Esteve, Leonardo Barrios

▶ **To cite this version:**

Maria Kitsara, Andreu Blanquer, Gonzalo Murillo, Vincent Humblot, Sara de Bragança Vieira, et al.. Permanently hydrophilic, piezoelectric PVDF nanofibrous scaffolds promoting unaided electromechanical stimulation on osteoblasts. Nanoscale, 2019, 11 (18), pp.8906-8917. 10.1039/C8NR10384D . hal-02351810

HAL Id: hal-02351810

https://hal.sorbonne-universite.fr/hal-02351810v1

Submitted on 6 Nov 2019

HAL is a multi-disciplinary open access archive for the deposit and dissemination of scientific research documents, whether they are published or not. The documents may come from teaching and research institutions in France or abroad, or from public or private research centers.

L'archive ouverte pluridisciplinaire **HAL**, est destinée au dépôt et à la diffusion de documents scientifiques de niveau recherche, publiés ou non, émanant des établissements d'enseignement et de recherche français ou étrangers, des laboratoires publics ou privés.

Please do not adjust margins

Nanoscale

ARTICLE

Permanently Hydrophilic, Piezoelectric PVDF Nanofibrous Scaffolds Promoting Unaided Electromechanical Stimulation on Osteoblasts

Received 00th January 20xx,
Accepted 00th January 20xx

DOI: 10.1039/x0xx00000x

www.rsc.org/

Maria Kitsara,*[a,d] Andreu Blanquer,[a,b] Gonzalo Murillo,[a] Vincent Humblot,[c] Sara De Bragança Vieira,[a] Carme Nogués,[b] Elena Ibáñez, [b,] Jaume Esteve,[a] and Leonardo Barrios*[b]

Biomimetic functional scaffolds for tissue engineering should fulfil specific requirements concerning structural, bio-chemical and electro-mechanical characteristics, depending on the tissue that they are designed to resemble. In bone tissue engineering, piezoelectric materials based on poly(vinylidene fluoride) (PVDF) are on the forefront, due to their inherent ability to generate surface charges under minor mechanical deformations. Nevertheless, PVDF's high hydrophobicity hinders sufficient cell attachment and expansion, which are essential in building biomimetic scaffolds. In this study, PVDF nanofibrous scaffolds were fabricated by electrospinning to achieve high piezoelectricity, which was compared with drop-cast membranes, as it was confirmed by XRD and FTIR measurements. Oxygen plasma treatment of the PVDF surface rendered it hydrophilic, and surface characterization revealed a long-term stability. XPS analysis and contact angle measurements confirmed an unparalleled two-year stability of hydrophilicity. Osteoblast cell culture on the permanently hydrophilic PVDF scaffolds demonstrated better cell spreading over the non-treated ones, as well as integration into the scaffold as indicated by SEM cross-sections. Intracellular calcium imaging confirmed a higher cell activation on the piezoelectric electrospun nanofibrous scaffolds. Combining these findings, and taking advantage of the self-stimulation of the cells due to their attachment on the piezoelectric PVDF nanofibers, a 3D tissue-like functional self-sustainable scaffold for bone tissue engineering was fabricated.

Introduction

Bone tissue engineering involves the development of cellularized scaffolds that can recapitulate natural bone properties.[1] One of the inherent properties of bone is piezoelectricity, which was reported back in 1957 by Fukada and Yasuda.[2] Their study revealed that the piezoelectricity in bone is attributed to the piezoelectric effect of the crystalline micelle of collagen molecules, thus to the extracellular matrix of cells and not to the cells themselves. Therefore, the development of scaffolds with piezoelectricity that mimic the extracellular matrix is highly desirable for bone regeneration, which can be reinforced from charges induced by mechanical stress. Taking into account the pivotal role of electrical stimulation in the functionality of living tissues[3], piezoelectric materials are promising candidates to be applied in injured tissues due to their ability to deliver an electric stimulus without the need for an external power source.[4,5]

In addition, a functional scaffold in tissue engineering should resemble the structural characteristics of the native microenvironment, thus the fibrous morphology of the extracellular matrix of most tissues. Amongst different fabrication techniques[6], electrospinning is the most effective method for the development of scaffolds with both fibrous structure and piezoelectricity in a single step.[7] During electrospinning, a high voltage is applied between the syringe needle tip, which contains a polymeric solution, and a grounded collector. Then, a nanofibrous network is created on the collector, which has been utilized for different tissue engineering applications.[8,9] In the case of piezoelectric polymers, nanofibrous piezoelectric scaffolds can be obtained by controlling the electrospinning parameters. The most studied piezoelectric polymer is poly(vinylidene fluoride) (PVDF)[10], and its increasing research interest stems from its fascinating properties due to the high electrical dipole moment.[11] Out of the five crystalline phases of PVDF, the most explored ones are the α, β and γ phases. While α phase is non polar due to the antiparallel packing of the dipoles in the unit cell, β phase possesses the highest electroactivity, followed by γ phase. Various methods have been reported in the literature for obtaining high piezoelectricity, where one of the most common is

[a] Instituto de Microelectrónica de Barcelona, IMB-CNM (CSIC), Bellaterra, 08193, Spain. Email: maria.kitsara@upmc.fr, kitsara.m@gmail.com
[b] Department de Biologia Cel·lular, Fisiologia i Immunologia, Universitat Autònoma de Barcelona, Bellaterra, 08193, Spain. Email: Lleonard.Barrios@uab.cat
[c] Sorbonne Université, Laboratoire de Réactivité de Surface UMR CNRS 7197, Paris, 75005, France
[d] Present Address: Sorbonne Université, Institut de Biologie Paris-Seine UMR CNRS 8256, Paris, 75005, France

† M.K. and A.B. contributed equally to this work.

Electronic Supplementary Information (ESI) available: ESI includes additional experimental details and figures including the scaffolds characterization and the long-term viability of Saos-2 cells cultured on them (PDF). It also includes three movies: CLSM z-stack of actin fibers in Saos-2 cells cultured on hydrophilic electrospun PVDF, and calcium transients of Saos-2 cells cultured on hydrophilic electrospun PVDF and on glass control (AVI). See DOI: 10.1039/x0xx00000x

Please do not adjust margins

Please do not adjust margins

poling under a strong electric field.[11,12] The comparative advantage of electrospinning is that piezoelectricity can be achieved in situ during the nanofibrous network formation, which is favorable in tissue engineering.

However, one of the drawbacks of PVDF is its inherent hydrophobicity that does not allow efficient cell attachment and expansion. A variety of methods have been reported in the literature for the surface modification of hydrophobic polymers.[13] Graft copolymerization and chemical vapour deposition (CVD) polymerization are two typical methods that were employed for PVDF surface functionalization.[14] Modification solely with plasma is another effective method for altering the surface properties of polymers that has been widely utilized in numerous studies and applications, but it has not yet been applied to PVDF porous scaffolds for their use in tissue engineering.[15–19] Plasma is considered as one of the best tools to modify polymeric surfaces homogeneously, and with no need for further specialized equipment or additional steps, along with the versatility of the effects that different plasmas have on polymeric surfaces in terms of chemistry and topography.

Aiming at improving surface wettability of piezoelectric PVDF scaffolds and ultimately achieving enhanced lifetime, we herein effectively employed this surface modification strategy in our scaffolds. We combined the advantages of both electrospinning and plasma treatment, and developed a novel scaffold for bone applications with promising properties, which was able to activate excitable cells, such as osteoblasts. In particular, we explored the effect of electromechanical stimulation on Saos-2 cells, upon growth on electrospun PVDF scaffolds.[20] Accordingly, electrospun PVDF nanofiber-based scaffolds were compared with PVDF scaffolds obtained by drop-casting. Our results have shown that the scaffolds remained stably hydrophilic for a long period of time (2 years after plasma treatment), and that the culture of Saos-2 cells on them led to a clear enhancement of their phenotype in comparison to their hydrophobic counterparts. The intracellular calcium dynamic measurements, using fluorescent calcium indicators, revealed a considerable increase of calcium transients in Saos-2 cells grown on electrospun scaffolds, demonstrating their electromechanical activation. In overall, our study proposes that the combination of electrospinning and oxygen plasma treatment of PVDF leads to the fabrication of a stable functional scaffold for bone tissue engineering.

Results and discussion

Surface-modified electrospun PVDF demonstrates favorable hydrophilicity and piezoelectric properties

Electrospinning of PVDF has been reported in a considerable number of studies, proposing different electrospinning parameters for obtaining higher piezoelectricity. In specific, the importance of parameters such as PVDF solution concentration, solvent system, electrospinning temperature, voltage, flow rate, distance from the tip to the collector have been extensively studied in the last decade.[12,21,22] Martins et al. in an explanative review article presented an overview of the methods for obtaining PVDF with high electroactive phases, and how the latter can be determined by X-ray diffraction (XRD) and Fourier-transform infrared spectroscopy (FTIR).[11] Having as a guide the aforementioned studies, we optimized our fabrication protocol by using as solvent system dimethylformamide (DMF)/acetone at a ratio 40/60 for both electrospun and drop-cast scaffolds (Fig. 1). We found that high voltage (25kV) and PVDF concentration were essential for obtaining electrospun scaffolds without beads as it was evaluated by scanning electron microscopy (SEM) (Fig. 1c). In the case of the drop-cast scaffolds, we lowered the solution concentration to obtain scaffolds with a thickness similar to the electrospun ones. SEM measurements have shown that drop-cast scaffolds consisted of globular particles with a mean diameter of 1.5 μm, which were interconnected with thin nanofibrils (Fig. 1d, images at higher magnification are included in the Fig. S1†), thus forming a structure of high porosity. The globular structure was reported for samples that were dissolved in DMF[23], while the co-presence of a solvent of low boiling point such as acetone, aided in the pores formation due to its high evaporation rate.

Evaluation of PVDF's long-term hydrophilicity after surface modification by oxygen plasma. As it is aforementioned, even though PVDF possess high piezoelectricity and is ideal for applications involving electromechanical generation, in tissue engineering it should additionally fulfill the requirement of appropriate surface properties for the effective attachment and subsequent interaction with cellular populations. PVDF is a hydrophobic polymer with a water contact angle of 130° (Fig. 1e, g), thus leading to very poor water affinity[13], and rendering cell attachment limited and in a non-physiological manner. In this study we utilized oxygen plasma for modifying the surface of the scaffolds, having in mind its simplicity and accessibility as a common plasma etcher/cleaner can be used. Water contact angle measurements revealed that 2 min exposure under oxygen plasma (treatment conditions described in the Materials and Methods section) was sufficient for obtaining long-term stable hydrophilic surfaces (Fig. 1f, h). The surfaces rendered to superhydrophilic immediately after plasma treatment, and were subsequently stabilized to hydrophilic after one month (water contact angle of 35°), which did not change even 2 years after the treatment (Fig. S2†). Surface topography was slightly altered under these treatment conditions, as it can be observed in the SEM images of Fig. S3†.

This journal is © The Royal Society of Chemistry 20xx

Please do not adjust margins

Nanoscale

ARTICLE

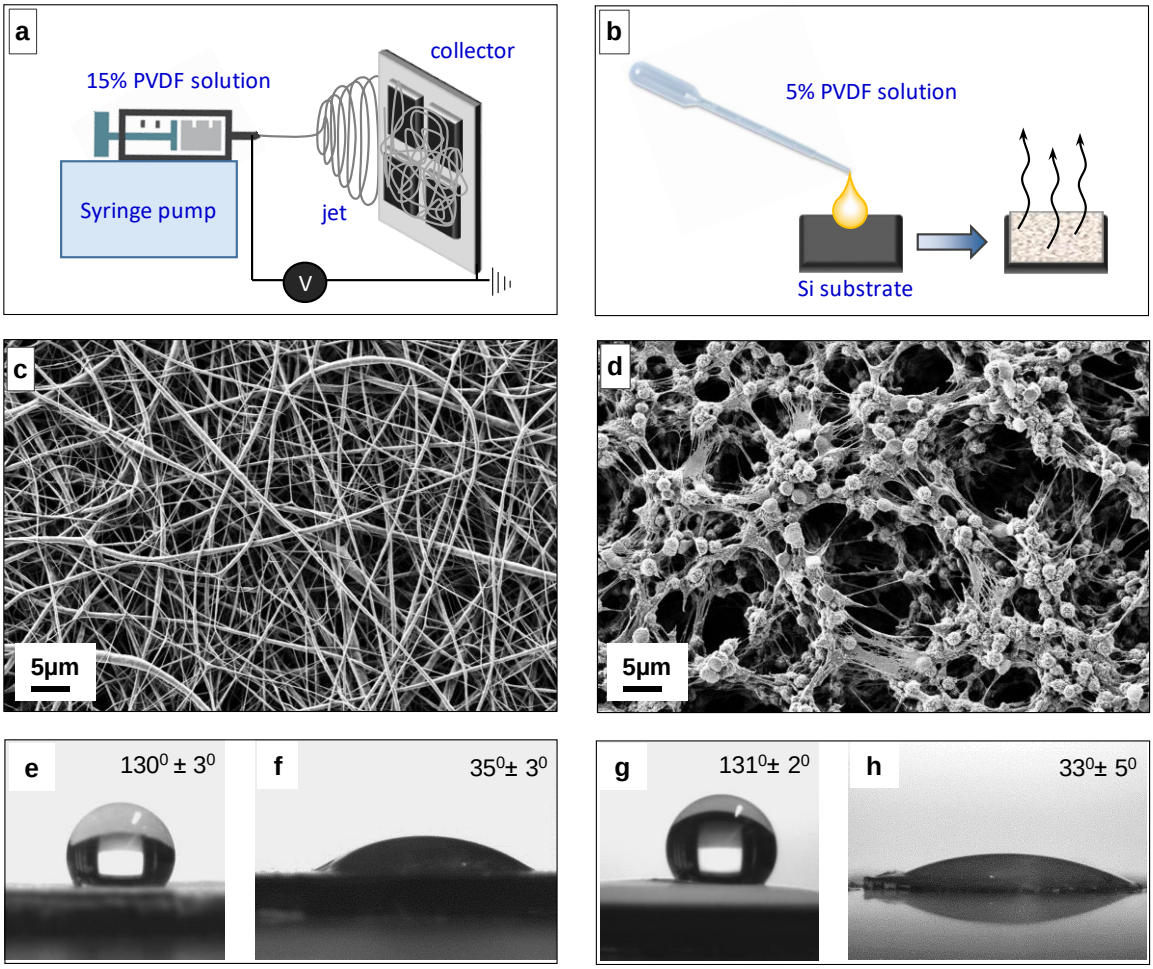

Fig. 1 Schematic representation of the process and photographs of the fabricated scaffolds: (a) electrospinning, (b) drop-casting. SEM images of (c) electrospun and (d) drop-cast scaffolds. Water contact angle measurements of PVDF scaffolds: (e, g) before and (f, h) after oxygen plasma treatment (e, f corresponds to electrospun and g, h to drop-cast scaffolds).

For scrutinizing this long-term hydrophilicity of plasma-modified scaffolds, we employed X-ray photoelectron spectroscopy (XPS) in order to identify the alterations in their surface chemical composition. The chemical composition of the hydrophobic (untreated) PVDF scaffolds is described in detail in the ESI, demonstrating the cleanliness of our scaffolds, which possess a negligible amount of oxygen in contrast to the most of the data reported in literature.[24,25] After plasma treatment, the main change observed on the survey spectrum, is the appearance of a feature associated with oxygen (O1s), representing 7.2 % of all atomic contribution (Table 2), which confirms the plasma activation process (Fig. S4†). Two main features are visible at 532.9 ± 0.1 eV and 534.4 ± 0.1 eV on Fig. 2e, named O_1 and O_2 and respectively assigned to oxygenated moieties bound to CF and CH groups in the first case, and COOH groups mainly in the second case (Table 1). Changes are also observed in the high-resolution spectra presented in Fig. 2; when looking at the C1s region (Fig. 2d) one can notice the appearance of the new feature, C_5 and C_6, in addition to the three already present before plasma treatment (C_1 to C_3). C_5 and C_6 features can be assigned to the degradation of the (CH_2-CF_2) backbone of PVDF due to plasma treatment, thus creating some oxygen radicals and new moieties, mainly -CFO-CH_2- and CF_2-CHOR- (Table 1). It is also important to emphasize that the plasma treatment and thus the degradation of the PVDF backbone is homogeneous through both CH_2 and CF_2 groups of the polymer, as the C_1:C_2 ratio remains stable at 0.94 (21.95:23.4) (Table 1). Finally, when looking at

Nanoscale

ARTICLE

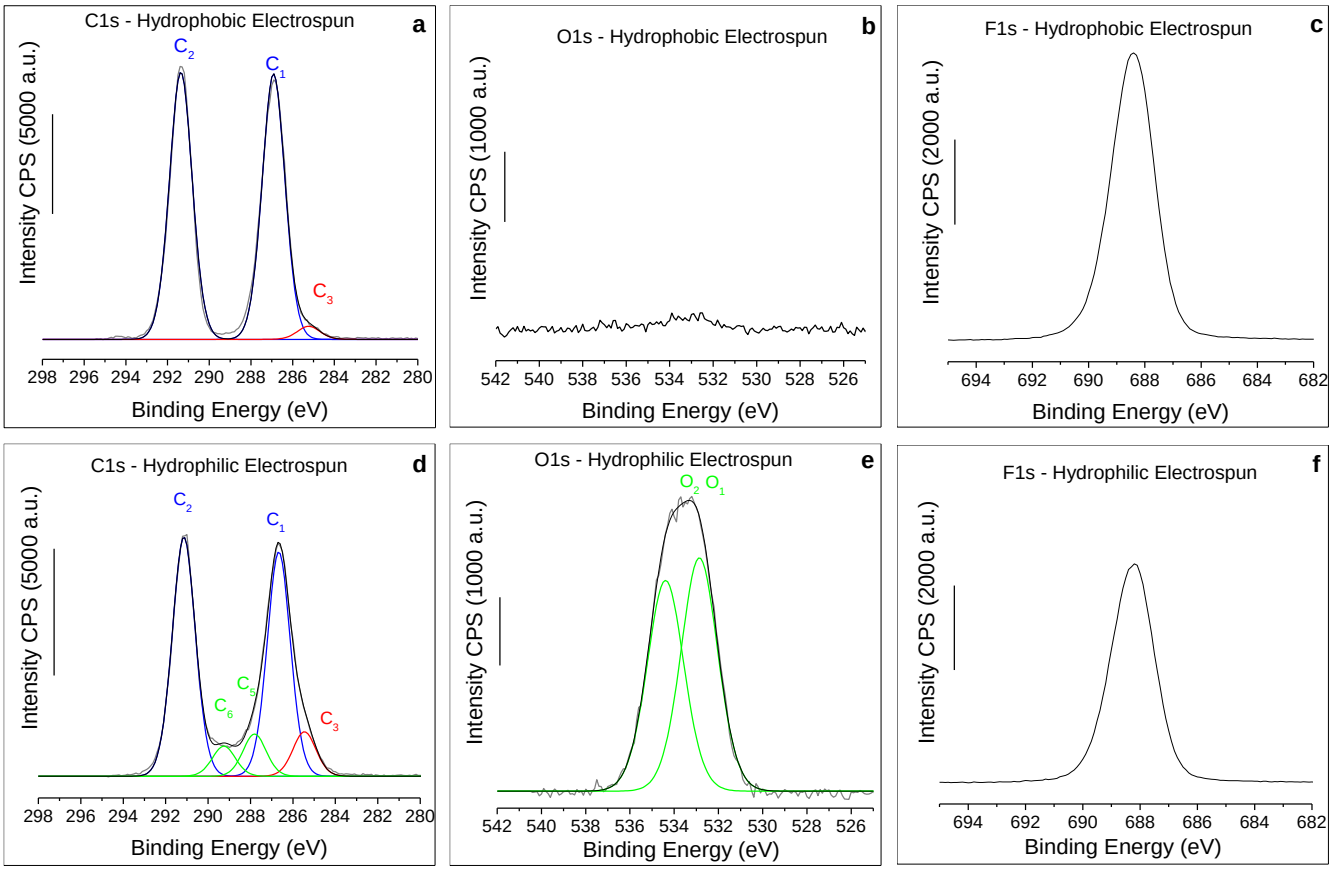

Fig. 2 C1s, O1s and F1s high resolution XPS spectra of electrospun PVDF before (a, b, c) and after plasma treatment (d, e, f).

the whole chemical composition of the membrane, before and after plasma treatment, one can see that the atomic percentage of carbon is stable (around 55%), whereas oxygen increases and fluorine decreases from 45% to 36% (Table 2). This is also accompanied with a decrease in the F/C ratio from 0.85 to 0.64 (Table 2), enabling to estimate a defluorination of roughly 25% of the PVDF scaffold, which is within the plasma activation process conditions efficiency.[17]

Table 1 Summary of binding energies (BEs) and functional groups from the high resolution XPS scan results of the PVDF scaffolds before and after oxygen plasma treatment.

		C1s						O1s		F1s
Scaffold		C_1	C_2	C_3	C_4	C_5	C_6	O_1	O_2	F_1
	Assign.	-CF_2-**C**H_2-	-**C**F_2-CH_2-	-**C**-C, -**C**-H	-CH=**C**F_2	-CF_2-**C**HO- -CF_2-**COOH**	-**C**-C=O(OH) -CF**O**-CH_2-	-C=**O**(OH) -CF_2-CH**O**- -CF**O**-CH_2-	-C=O(**O**H)	-CF_2-
Hydrophobic Drop-cast	BE (eV)	286.9	291.4	284.8	294.2	--	--	--	--	688.5
	Atomic %	25.3	26.4	0.7	1.25	--	--	0.5		45.85
Hydrophilic Drop-cast	BE (eV)	286.5	291.0	285.1	--	287.7	289.1	532.6	534.2	688.1
	Atomic %	21.9	23.6	2.5	--	4.2	3.0	4.1	3.2	37.5
Hydrophobic Electrospun	BE (eV)	286.9	291.4	285.0	--	--	--	--	--	688.4
	Atomic %	26.65	26.8	1.3	--	--	--	0.25		45.0
Hydrophilic Electrospun	BE (eV)	286.6	291.2	285.4	--	287.8	289.3	532.9	534.4	688.3
	Atomic %	21.95	23.4	4.35	--	4.15	2.95	3.9	3.5	35.8

This journal is © The Royal Society of Chemistry 20xx

Nanoscale

ARTICLE

In a second step, we have investigated any potential differences that the two scaffold fabrication methods could provoke. Data are presented before and after plasma treatment on Fig. S4† and S5†, and are summarized in Table 1 and 2. From the survey spectra, there is a high reproducibility between both hydrophobic and hydrophilic scaffolds (Fig. S4†). High resolution O1s and C1s region further confirmed this tendency, together with the atomic percentage and ratio showing very good correlation between both fabrication methods: 0.85 and 0.89 for the F/C ratio for the electrospun and drop-cast, respectively (Fig. S5†). After treatment, the O/C ratio is also very close between the electrospun (0.127) and the drop-cast samples (0.133), confirming the effectiveness of oxygen plasma treatment on PVDF scaffolds regardless of the fabrication method used.

Table 2 Summary of PVDF scaffolds atomic composition derived from XPS analysis.

Scaffold	Atomic composition %			Atomic Ratio	
	C1s	F1s	O1s	F/C	O/C
Hydrophobic Drop-cast	53.8	45.75	0.45	0.89	0.008
Hydrophilic Drop-cast	54.8	37.9	7.3	0.69	0.133
Hydrophobic Electrospun	54.55	45.25	0.20	0.85	0.004
Hydrophilic Electrospun	56.7	36.1	7.20	0.64	0.127

Assessment of electrospun PVDF scaffolds' piezoelectricity. The piezoelectric properties of the fabricated scaffolds were evaluated with XRD and FTIR spectroscopy. XRD diffractograms of all scaffolds show a broad peak a little bit higher than 20°, which results from the overlap of the peaks at 18.4° and 20.7° ascribed to α and β phases respectively (Fig. 3a).[26] However, it must be noted that in the area of 18.6° and 20.2°, peaks attributed to γ phase exist, which makes it difficult to clearly distinguish between β and γ phases.[11] Nevertheless, all electrospun scaffolds have a shift to slightly higher values in the area of 20.6°, which is translated to the strong presence of β phase. In addition, the shoulder at 18.7° is weaker in the case of the electrospun scaffolds, which further indicates that the transition from α to β phase occurred in higher extent in comparison to the drop-cast scaffolds, and that γ phase exists in lower extent. The diffractogram of as received PVDF powder presents the characteristic peaks ascribed exclusively to α phase at 18.3° and 19.9° and 26.6°, and served as a good control for the distinction between α and β/γ phases in our scaffolds.[27] The comparison of the drop-cast scaffolds with the powder shows clearly that the drop-cast scaffolds exhibit peaks characteristic to γ and β phases, but the characteristic peak attributed to α phase at 26.6° totally

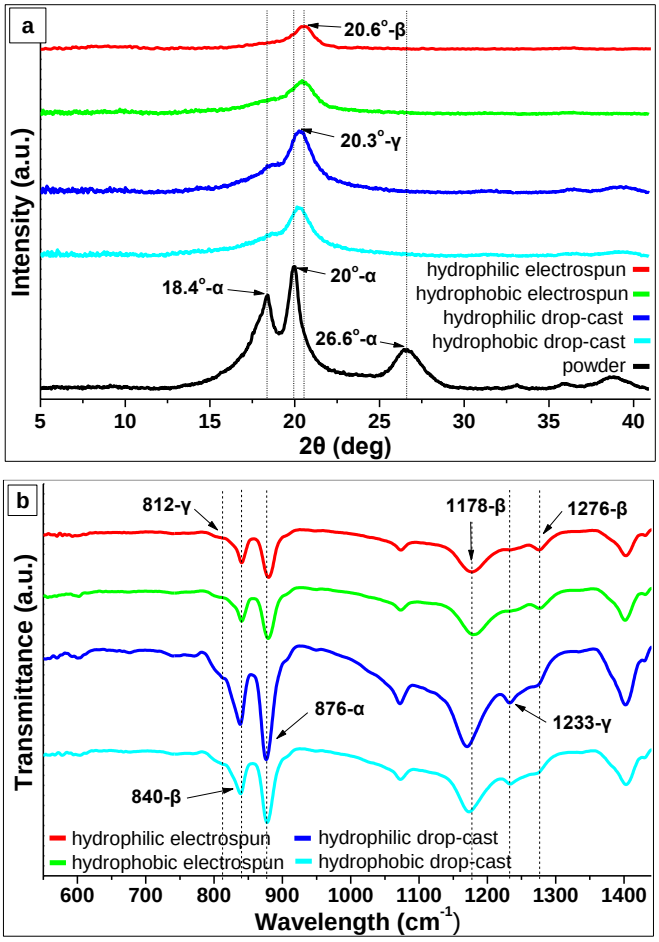

Fig. 3 (a) XRD diffractograms and (b) FTIR spectra of the fabricated PVDF scaffolds.

disappeared. Therefore, it is evident that there is a clear transition of α to β and γ phase in all scaffolds: electrospun scaffolds exhibit higher β phase while drop-cast higher γ phase.

FTIR spectra have shown that all scaffolds show a peak at 840 cm^{-1} that corresponds to CH_2 rocking/CF_2 asymmetrical stretching of β phase (Fig. 3b). Nevertheless, the same band is ascribed to γ phase too, which makes it again difficult to distinguish between these two phases.[11] The 812 cm^{-1} band is characteristic of γ phase and appears in all scaffolds, but in the case of the electrospun the shoulder is weaker.[11] Drop-cast scaffolds show a clear peak at 1233 cm^{-1}, characteristic of γ phase, whereas electrospun scaffolds have a peak at 1276 cm^{-1} which is attributed to C–F stretching vibrations of β phase. Additionally, electrospun scaffolds show a peak at 1177 cm^{-1} ascribed to β phase due to C-F characteristic stretching vibration, while for the drop-cast scaffolds the peak appears at 1170 cm^{-1}. Characteristic peaks of α phase such as 612, 763, 765, 796, 970, 976

This journal is © The Royal Society of Chemistry 20xx

Please do not adjust margins

cm^{-1} do not appear in any of the scaffolds, except from the intense peak at 876 cm^{-1} which is apparent in all of them.

One can conclude that drying of the drop-cast scaffolds at room temperature under a fume hood, which accelerated the solvent evaporation, and taking into account the higher proportion of the volatile acetone over DMF in the final solution, led to the transition of α to γ phase. The electrospinning process led to the transition of α to β phase at a higher extend, in comparison to the drop-cast scaffolds. The applied high voltage during the electrospinning process stretched the PVDF solution jet, and in combination with the high evaporation rate of acetone, led to the alignment of electric dipoles in the formed PVDF nanofibers. Summarizing, XRD and FTIR analyses revealed that even the scaffolds fabricated by the simple drop-casting method exhibit piezoelectric properties, but mainly attributed to the γ phase. On the other hand, there is a clear predominance of β phase in the electrospun scaffolds. In addition, there is no apparent difference between the samples before and after the treatment with oxygen plasma.

In addition, a flexible test device was fabricated in order to validate the piezoelectric properties of the electrospun scaffolds with electromechanical measurements. This test device consists of PVDF nanofibers directly deposited by electrospinning on a gold-coated thin plastic substrate, which was subsequently covered with an electrically conductive tape (Fig. S6†). Using this method, a cantilever-like structure was created, having a piezoelectric PVDF fibrous network sandwiched in between two electrodes. The device that was mounted on a high frequency shaker system, was submitted to a vibration with a certain acceleration and the frequency response was recorded (Fig. S6†). Due to the strain generated in the nanofibers by the cantilever's deflection at resonance, an open-circuit voltage peak of 0.6 V was measured. Although, this test device was not optimized as neither a sensor nor an energy generator, it allowed for practical demonstration of the piezoelectric nature of the electrospun PVDF scaffolds.

Hydrophilic PVDF scaffolds improve Saos-2 cells cytocompatibility

PVDF cytocompatibility has been reported by several authors using different cell types and different PVDF structures, thus demonstrating its efficacy as a promising material for biomedical applications.[28,29] Notwithstanding, only a few studies have analyzed in depth the cytocompatibility of electrospun PVDF scaffolds[27], and to the best of our knowledge there is no report scrutinizing the osteoblasts interaction with plasma-modified PVDF. For our biological experiments, we utilized the Saos-2 cell line. This cell line is derived from osteosarcoma and could show some differences in terms of cellular behaviour when compared with primary human osteoblasts. However, Saos-2 cells have been widely used to test the cytocompatibility of new developed materials for biomedical applications and are considered as a representative model of multiple osteoblasts responses.[30] Cytocompatibility analysis involves several biological parameters such as cell viability, adhesion and spreading. Saos-2 viability was determined after 3 days in culture on the surface of all samples. Quantification of live cells using the Live/Dead kit showed that the percentage of live cells was higher than 83% for all samples and no significant differences were observed among them (Fig. 4a). The number of cells grown on samples was quantified after three days in culture and no significant differences were observed (Fig S7†). Moreover, in order to demonstrate that cells were able to proliferate, and that PVDF scaffolds were not cytotoxic when used for longer periods, we additionally performed the same Live/Dead analysis after 14 and 30 days in culture. We observed that the scaffold surface covered by cells increased with culture time indicating their proliferation, and that after 30 days in culture the scaffolds were full of live cells (Fig. S8† and S9†), demonstrating the safety of the material over time. Cell viability results were in agreement with other studies that conclude PVDF is not cytotoxic and allow cell proliferation.[14,27]

Surface topography and wettability are two parameters that can modulate cell adhesion and cell spreading. For example, it has been described that cells grown on hydrogels or fibrous networks of methacrylated dextran with different stiffness show differences in spreading area and proliferation.[31] Spreading areas of Saos-2 cells grown on PVDF samples were measured after 3 days in culture (Fig. 4b). The results revealed that osteoblasts adhesion on PVDF samples was significantly improved in the hydrophilic ones, exhibiting spreading areas about two-fold the areas of the cells cultured on the non-treated hydrophobic scaffolds. Cells grown on glass coverslip controls showed the highest values of spreading area. These results of cell spreading are in agreement with previous studies that concluded that high contact angles (> 90°) are associated with poor cell adhesion, whereas low contact angles (< 90°) are associated with good cell adhesion and spreading.[32–34]

Saos-2 cells interaction with PVDF and the shape of Saos-2 cells growing on PVDF samples were analyzed after 3 days in culture using SEM and confocal laser scanning microscopy (CLSM). Cell morphology analysis by SEM indicated that cells grown on the hydrophilic surfaces showed a polygonal shape with thin and long filopodia (Fig. 4d, f). However, cells grown on hydrophobic surfaces presented a rounded shape without extended cytoplasmic projections (Fig. 4c, e). When grown on hydrophilic electrospun PVDF scaffolds, adhered Saos-2 cells were in close contact with the nanofibers, showing a shape adapted to the topography and the distribution of nanofibers. This adapted morphology was not observed in cells growing on hydrophobic electrospun PVDF scaffolds. Furthermore, we employed focused ion beam (FIB) for cutting the samples vertically, and the SEM images confirmed the very tight interaction between osteoblasts and hydrophilic scaffolds. In addition, cells seemed to start migrating into the hydrophilic PVDF nanofibrous mesh, and the latter enfolded them to create a tissue-like structure, in contrast to the hydrophobic ones where cells rested only on top of them (Fig. 4g, h). Summarizing, SEM results are in agreement with the spreading area results, where stretched cells were observed on the hydrophilic samples.

 This journal is © The Royal Society of Chemistry 20xx

Please do not adjust margins

Nanoscale

ARTICLE

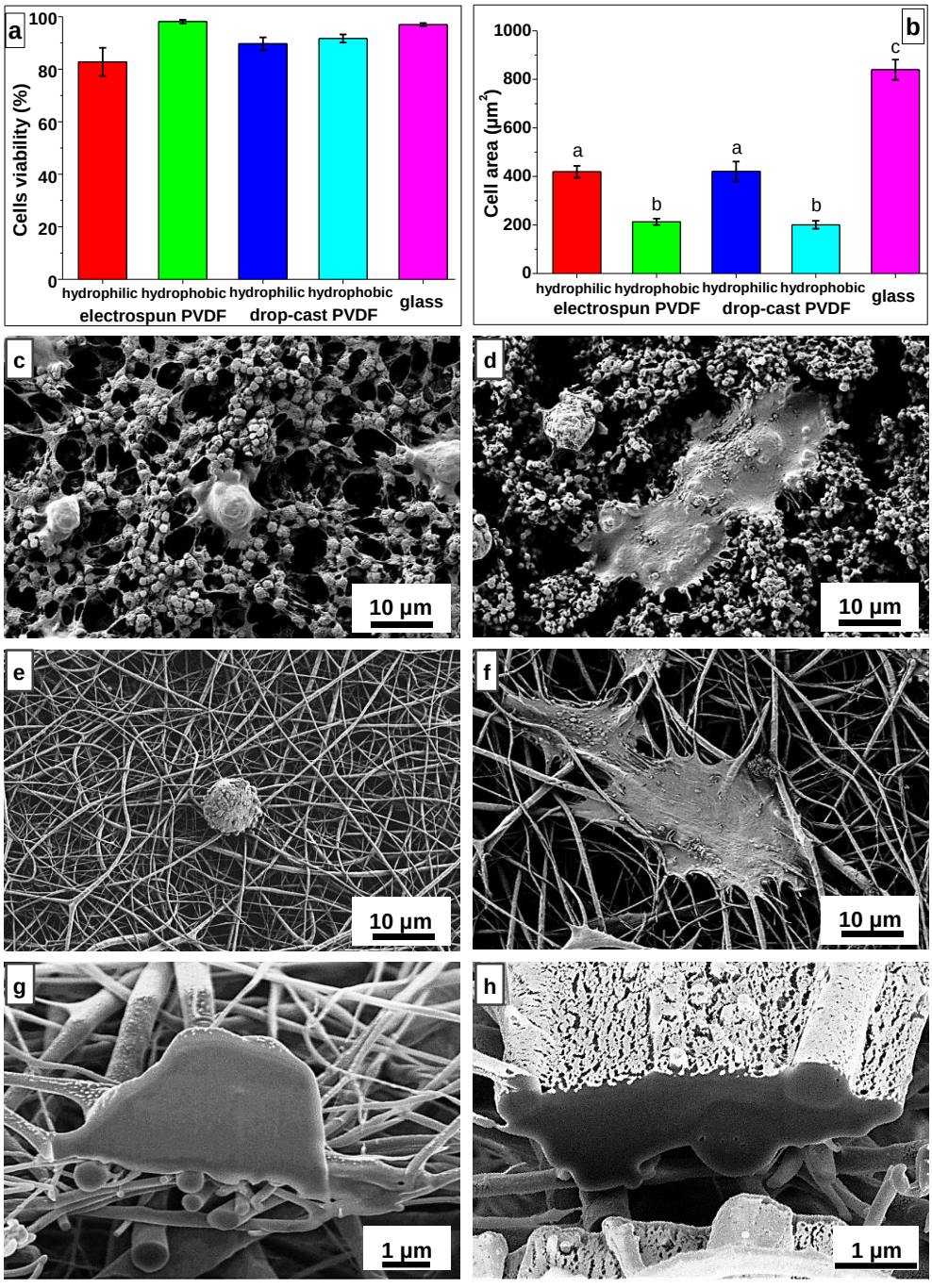

Fig. 4 Saos-2 cells cultured on PVDF samples and control glass coverslips: (a) viability, (b) spreading area. No significant differences were observed for the viability test (Kruskal-Wallis test with Dunn's multiple comparisons), and for the spreading area measurements (one-way analysis of variance, ANOVA, with Bonferroni multiple comparison test). Different letters above the columns indicate significant differences. SEM images of the cultured Saos-2 cells on: (c, d) hydrophobic and hydrophilic PVDF drop-cast, (e, f) hydrophobic and hydrophilic PVDF electrospun scaffolds respectively. (g, h) SEM-FIB cross-sections of Saos-2 cells grown on hydrophobic and hydrophilic electrospun scaffolds respectively.

This journal is © The Royal Society of Chemistry 20xx

Nanoscale

ARTICLE

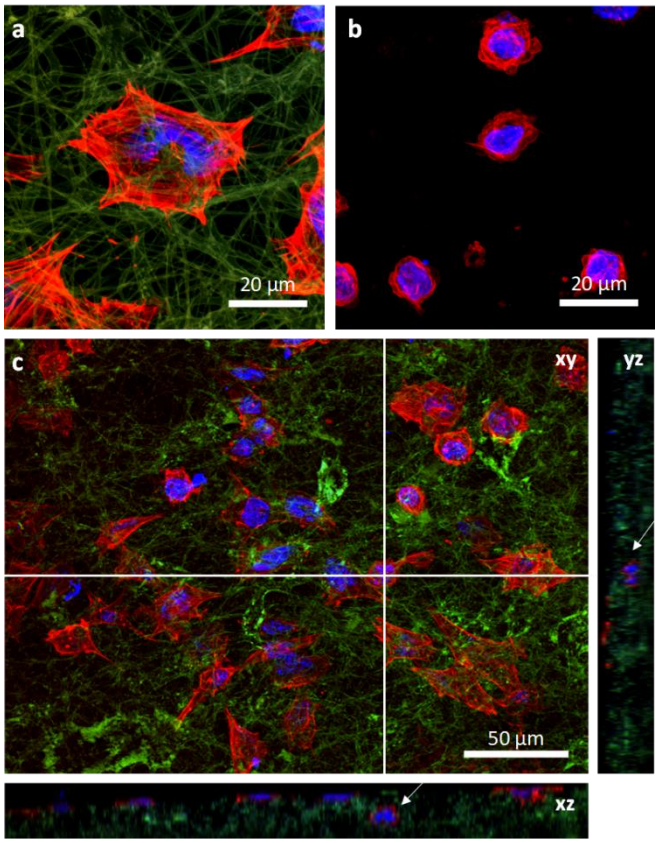

The CLSM analysis of cells grown on hydrophilic electrospun PVDF scaffolds showed well defined actin stress fibers crossing the cell from end to end, whereas cells cultured on the hydrophobic ones presented short and disrupted actin bundles (Fig. 5a and b). The orthogonal projection of Saos-2 cells growing on hydrophilic PVDF demonstrated that cells are inserted into the hydrophilic nanofibrous mesh which probably indicates their capacity to migrate (Fig. 5c). Cell interaction with PVDF scaffolds and cell migration into the scaffolds

Fig. 5 Saos-2 cells cultured on (a) hydrophilic and (b) hydrophobic electrospun PVDF scaffolds for 3 days. (c) Orthogonal projection of Saos-2 cells grown on and between hydrophilic PVDF nanofibers. Actin fibers (red), nuclei (blue) and auto-fluorescent hydrophilic PVDF fibrous mesh can be observed.

are essential parameters for their use in regenerative medicine applications. Scaffold surface properties play a key role in tissue integration, an indispensable factor for reducing the risk of implant loosening.[35] Thus, rendering PVDF scaffolds hydrophilic with a simple oxygen plasma treatment proved to be highly efficient for improving cell attachment, expansion and proliferation.

PVDF piezoelectricity due to electrospinning induces intracellular calcium elevation in Saos-2 cells

The osteoblasts' response when grown on piezoelectric PVDF scaffolds was analyzed by evaluating the changes in intracellular calcium concentration over time. Calcium is involved in several intracellular pathways, and acts in signal transduction upon activation of ion channels.[36,37] The concentration of intracellular calcium is related to calcium ions entering the cytoplasm via plasma membrane channels, such as voltage-gated calcium channels (VGCC) and stretch-activated calcium channels (SACC), or from internal calcium stores in the endoplasmic reticulum (ER).[38,39] The plasma membrane depolarization due to the electric field opens the VGCC and SACC, that would produce high amplitude calcium transients for several seconds. In osteoblasts, the depolarization potential values are in the range of 30 mV. [40] On the other hand, short time and very low amplitude calcium changes are due to intracellular pathways.[41]
It has been reported that Saos-2 cells exposed to direct current electric fields were subjected to changes in their cytoplasmic calcium concentration.[42] Regarding piezoelectric materials, it was proven that ultrasound-driven piezoelectric stimulation was able to induce calcium influx in neurons, which mediated the enhancement of neurite outgrowth and neural differentiation.[43] In our study we observed that osteoblasts grown on electrospun PVDF scaffolds showed intracellular calcium concentration transients (44% on hydrophilic scaffolds and 46% on hydrophobic scaffolds), whereas very few cells presented these transients on PVDF drop-cast samples (15% on hydrophilic samples and 18% on hydrophobic samples), and on glass control (5%) (Fig. 6a-c). Fig. 6b shows two characteristic calcium influx patterns, which represent the majority of patterns obtained by cells grown on hydrophilic electrospun scaffolds and glass control. In overall, the number of activated cells (with calcium transients) did not present significant differences regarding wettability for both electrospun and drop-cast samples, even though cell-material interactions (cell morphology and spreading area) were different depending on PVDF wettability, as observed with SEM and CLSM. This result is in agreement with the XRD and FTIR measurements, which have indicated that the piezoelectricity is not affected by the plasma treatment.
The present results suggest that piezoelectric PVDF scaffolds are able to generate a local electric field that activates the osteoblasts (Fig. 6d). Cells grown on electrospun scaffolds, adhere to them, and consequent generate adhesion forces[44], which are probably able to bend the PVDF nanofibers. Thus, we hypothesize that the mechanical stress produced by cells adhesion is responsible for the electromechanical stimulation of themselves, which is in accordance with the piezoelectric capacity of electrospun scaffolds. In this regard, the response varies from cell to cell due to the different interactions with nanofibers, the nanofibers geometry, and the cell status. These results are in agreement with our simulations (fig. S10†), where a maximum piezopotential of 30mV can be obtained by a single PVDF nanofiber when strained with a magnitude similar to

This journal is © The Royal Society of Chemistry 20xx

Please do not adjust margins

this produced by a cell (0.1–10 nN). [45,46] This voltage value seems to be enough to electrically stimulate the VGCCs present in the cell membrane and therefore this nanofiber-cell interaction allows the electrical stimulation of the cell, as demonstrated in our previous work. [47]

Several papers have analyzed the cytocompatibility of piezoelectric polymers and the response of different cell types to electromechanical stimulus.[5,28] In the present paper, we demonstrate that osteoblasts, when interacting with the PVDF scaffolds, are activated without the need for external stimuli to induce the piezoelectric response. These results are in agreement with previous studies of our group in which we analyzed the osteoblasts interaction with zinc oxide (ZnO) piezoelectric nanogenerators and their self-stimulation.[47] ZnO nanosheets were also able to generate a local electric field in response to the forces of adhered osteoblasts, which was in the basis of the intracellular calcium transients induction. Both ZnO nanosheets and PVDF scaffolds are cytocompatible and piezoelectric, and can be used for the electromechanical stimulation of excitable cells. Nevertheless, the hydrophilic electrospun PVDF scaffolds combine advanced cell adhesion, spreading and migration into the fibrous mesh, with cell activation due to an induced electrical stimulation. Hence, electrospun surface-modified PVDF scaffolds' superiority lies in their morphology, which resembles that of the extracellular matrix. By following this route, 3D tissue-like structures can be achieved, expanding the range of applications in regenerative medicine.

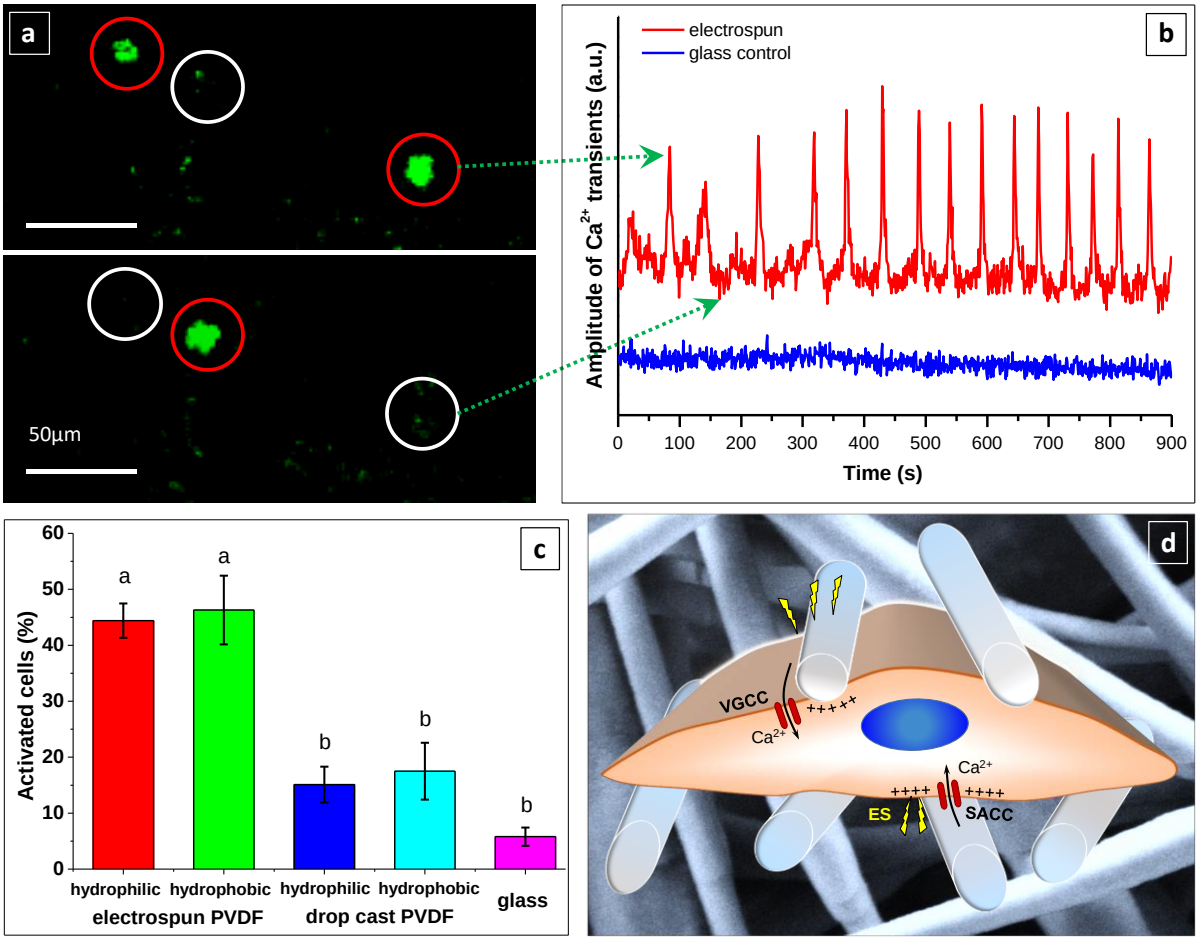

Fig. 6 (a) Snapshots of images showing changes in Ca^{2+} fluorescence intensity at different time frames; red circles enclose activated cells in the On mode (Ca^{2+} fluorescence intensity elevation) and white circles in the Off mode. (b) Ca^{2+} influx pattern of characteristic cells grown on hydrophilic electrospun scaffolds (red line) and the control glass coverslip (blue line). (c) Percentage of activated cells grown on different PVDF scaffolds. Different superscripts on top of the columns denote significant differences ($p<0.05$) among the different structures and wettability. (d) Schematic representation of a cell cultured on hydrophilic electrospun PVDF scaffold; electrical stimulation (ES), coming from the 3D fibrous scaffold' bending due to the cell forces applied upon attachment, causes the opening of plasma membrane channels (VGCC, SACC) which lead to an increase of calcium ions in the cytoplasm.

Experimental

Scaffolds fabrication

PVDF powder (M.W. 534 K), DMF and acetone was purchased from Sigma-Aldrich. For the formation of the electrospun scaffolds, a commercial instrument from Bioinicia was used (Fluidnatec® LE-10). A PVDF solution of 15% in DMF/acetone (40/60) was loaded into a syringe which was connected with a

Please do not adjust margins

Please do not adjust margins

nozzle tip of 0.9 mm outer diameter, while the flow rate was controlled via a pump at 600 µl/h. The distance between the nozzle tip and the grounded collector was fixed at 15 cm. Pieces of silicon wafer with dimensions 6×6 mm^2 were stuck on the collector which were used as substrates for the cell culture. By applying voltage as high as 25 kV for 20 min, a mesh of nanofibers was successfully deposited to the silicon substrates at room temperature (20±2°C) (Fig. 1a, c). The scaffold thickness, measured by a stylus profilometer from Tencor Instruments, was 17 ±3 µm. Afterwards, the samples were let to dry overnight at room temperature (RT). For the formation of the drop-cast samples, PVDF solution of 5% in the same solvent system was cast on the same silicon substrates as those used for the electrospun scaffolds (Fig. 1b, d). The samples were let to dry under a fume hood for 2 days at RT.

Scaffolds surface treatment

Both electrospun and solvent cast scaffolds were treated with oxygen plasma for achieving a hydrophilic surface. The microwave plasma etcher Tepla 300E was utilized under the following conditions: 200W, 0.8 mbar, gas flow of 50 sccm O_2, for 2min.

Scaffolds characterization

SEM was used to visualize the structure of the generated scaffolds using an Auriga (Carl Zeiss) system. The samples were sputtered with a thin gold layer prior to SEM observation (Bio-Rad Polaron Division SEM Coating System). Images at different magnifications were obtained on at least five different areas in the same sample and in three different samples with the same conditions. The images were performed by applying beam voltage of 1-2 kV and using InLens detector.

Water contact angle measurements were performed using the DSA 100 system from Krüss. The sessile drop method was used and the measurements took place at 20°C. The volume of the applied drops of deionized water was 1.5 µl. Contact angle data were obtained by averaging over several measurements in different areas on the samples surface.

XPS analyses were performed using an Omicron Argus X-ray photoelectron spectrometer, equipped with a monochromated AlK_α radiation source ($h\nu$ = 1486.6 eV) and a 300 W electron beam power. The emission of photoelectrons from the sample was analyzed at a takeoff angle of 90° under ultra-high vacuum conditions (≤ 10^{-10} Torr). Spectra were carried out with a 100 eV pass energy for the survey scan and 20 eV pass energy for the C1s, O1s, N1s, S2p regions. Binding energies were calibrated against the $Au4f_{7/2}$ binding energy at 84.0 eV and element peak intensities were corrected by Scofield factors.[48] The peak areas were determined after subtraction of a linear background. The spectra were fitted using Casa XPS v.2.3.15 software (Casa Software Ltd., U.K.) and applying a Gaussian/Lorentzian ratio G/L equal to 70/30.

XRD patterns of the samples were collected on a Bruker D8 Advance diffractometer (source: CuKα, λ=1.54 Å) equipped with a bidimensional General Area Detector Diffraction System (GADDS) detector. A 2θ angle ranging from 5.5° to 41°, a voltage of 40 KV and a current of 40 mA were used.

FT-IR spectroscopy was performed under attenuated total reflectance (ATR)-FTIR mode using the universal ATR accessory (U-ATR) of the Perkin-Elmer Spectrum One spectrometer. The measurements were carried out in transmittance mode from 550 to 4000 cm^{-1} with 1 cm^{-1} resolution and total of 40 scans at 20°C.

Test device fabrication and electromechanical characterization

A flexible test device was fabricated by placing the electrospun PVDF scaffold in between two electrodes (Fig. S6†). Specifically, the scaffold was directly electrospun on a conductive substrate in order to ensure a full coverage and full contact. The substrate consisted of a cyclic olefin polymer film (COP) of 188 µm thickness coated with a thin gold layer (100 nm). Then the scaffold was covered with an electrically conductive tape which worked as the upper electrode.

In order to generate a specific vibration, a set-up composed of a high-frequency shaker VR5200HF and a controller VR9500, from Vibration Research, was used. A low-noise voltage preamplifier, SR570, was utilized to obtain high load impedance (100 MΩ). The sample was glued to the base of the shaker to create a cantilever-like structure. Then a sweep in frequency (from 10 Hz to 20 Hz) was performed maintaining a constant acceleration (0.2G). The electrical current generated by piezoelectricity when the sample was at resonance was acquired with the input port of the VR9500 controller through the SR570 preamplifier.

Cell culture and viability assay

Human osteosarcoma Saos-2 cells (ATCC) were cultured in Dulbecco's modified Eagle's medium (DMEM, Invitrogen) with 10% foetal bovine serum (FBS, Life Technologies) under standard conditions (37°C and 5% CO_2). Cell culture glass coverslips were used as controls (purchased from Waldemar Knittel). The PVDF samples and glass coverslips were introduced into a 4-multiwell culture plate and sterilized by UV light for at least 2 h. Once sterilized, 50,000 cells were seeded into each well and cultured for 3 and 30 days. Cell viability was evaluated using the Live/Dead Viability/Cytotoxicity kit for mammalian cells (Invitrogen), according to the manufacturer's protocol. Images from different randomly selected regions from all samples and controls were captured using an Olympus IX71 inverted microscope equipped with epifluorescence. For each analysis a minimum of 300 cells were scored. The experiment was performed in triplicate.

Spreading area measurements

To quantify the mean spreading area per cell, the spreading area of cells adhered onto PVDF and control surfaces was quantified using the images previously captured for cell viability assay. The cell spreading area of live cells was measured analysing fluorescent calcein using Image J software. For each experiment (n=3), three different regions were analyzed.

Cell morphology and adhesion analysis

The same samples used for the assay of viability were processed for SEM and FIB analysis. Cells were washed in phosphate buffered saline (PBS), fixed in 4 % paraformaldehyde in PBS for 15 min at RT and washed again in PBS. Cell dehydration was performed in a series of increasing ethanol concentrations (50, 70, 90 and twice 100%) for 8 min each. Finally, samples were dried using hexamethyldisilazane (Electron Microscope Science) for 15 min. Samples were mounted on special stubs and analyzed using a SEM (Zeiss Merlin) in order to

 This journal is © The Royal Society of Chemistry 20xx

Please do not adjust margins

Please do not adjust margins

observe cell morphology. In addition, samples were cut using FIB in order to better observe the interaction between cells and piezoelectric scaffolds.

Cytoskeleton organization was assessed by actin fibers detection. Following the same protocol described for the viability assay, cells were seeded onto samples and, after 3 days, cells were fixed in 4% paraformaldehyde in PBS for 15 min at RT. Then, samples were incubated with a mixture of Texas Red-conjugated phalloidin and Hoechst 33258 (both from Invitrogen) for 30 min at RT. Finally, cells were washed in PBS, air dried and mounted on a specific bottom glass dishes (MatTek) using ProLongAntifade mounting solution (Life Technologies). Samples were analyzed in a CLSM (Olympus XT7).

Intracellular calcium quantification

CLSM (Leica SP5) was used to detect the intracellular calcium increase over time. Saos-2 cells were cultured on samples for 24 h in standard conditions, then cells were loaded with 2 µM Fluo-4 AM and 0.02% pluronic acid (both from Life Technologies) in serum free DMEM for 30 min in the dark at RT. Samples were washed with serum-free DMEM and then transferred to MatTek dishes with fresh medium. Images of osteoblasts were captured every 1 sec during 15 min. Changes in fluorescence intensity during the time of monitoring were processed using Image J software. A MATLAB code was developed to automatically detect fluorescent changes in the intracellular calcium of the cells, taking the time-lapse movies recorded in the CLSM as data source. Several image enhancement routines and a perimeter detection algorithm were used to detect all the cultured cells. Then, mean relative intensity along time was calculated for each particular cell, using an automatic suitable threshold for every different measurement. Finally, every cell relative intensity was used as input of an ad-hoc peak detector to estimate whether the cell was activated by the scaffolds. As a result, the signals of relative fluorescence intensity (i.e. relative calcium concentration) versus time were acquired for each cell.

Statistical analyses

The quantitative data is presented as mean ± standard error (SE). Statistical comparisons were performed using Kruskal-Wallis test with Dunn's multiple comparisons for cell viability assay. The one-way analysis of variance (ANOVA) with Bonferroni multiple comparison test was used for the spreading area assay. The number of activated cells were analyzed using the Kruskal-Wallis test with Tukey's comparison. In all cases, the analysis was performed using GraphPad Prism. Statistical significance was considered when $p < 0.05$.

Conclusions

In this study, we employed electrospinning and plasma post-modification for obtaining PVDF nanofibrous scaffolds that combine favorable electromechanical properties and enhanced wettability. Their efficacy as potential tissue engineering constructs was evaluated using osteoblast-like cells. Our results revealed that the β phase of PVDF is predominant in electrospun scaffolds while the γ phase appears higher in the drop-cast scaffolds, which served as controls. Post-treatment with oxygen plasma modified the PVDF scaffolds' surface chemistry and improved their wettability, as it was validated by XPS and contact angle measurements. It is the first time that a two-year long-term stable hydrophilicity is reported in this kind of scaffolds when plasma functionalization is used, which opens the repertoire of their applications in tissue engineering and regenerative medicine, where long-term cell cultures as well as implants with enhanced lifetime are a prerequisite in many cases. In order to demonstrate the suitability of the surface-modified piezoelectric PVDF scaffolds for bone tissue engineering, we have cultured Saos-2 cells on them. All the scaffolds exhibited excellent cytocompatibility, but the hydrophilic ones led to an improved osteoblast phenotype as demonstrated by cell spreading. In addition, the highly piezoelectric electrospun scaffolds induced intracellular calcium transients, as quantified by the number of activated cells. The drop-cast PVDF activated less cells comparing to the electrospun equivalent, yet still more than double than the glass control, indicating that they possess a low degree of piezoelectricity that is mainly attributed to γ phase. In conclusion, the combination of a highly β-phase electrospun PVDF with oxygen plasma treatment can result in a functional and stable hydrophilic scaffold, which can stimulate excitable cells, like osteoblasts, without the need of an external power source. These findings can lead to new venues in tissue engineering, based on biomimetic 3D scaffold-electromechanical stimulation fashion.

Conflicts of interest

There are no conflicts to declare.

Acknowledgements

The authors would like to thank Anna Crespi for performing the XRD measurements and the staff at the Servei de Microscòpia of Universitat Autònoma de Barcelona. This study was supported by the Spanish Government (MAT2017_86357-C3-3-R and TEC2015-72461-EXP), Generalitat de Catalunya (2017-SGR-503) and the EU project EnSO (H2020-ECSEL-JU). MK acknowledges funding through the Beatriu de Pinós program (BP-DGR-2013), supported by the Secretary for Universities and Research of the Ministry of Economy and Knowledge of the Government of Catalonia and the Cofund programme of the Marie Curie Actions of the 7th R&D Framework Programme of the European Union. Also, the authors acknowledge IMPC (Institut des Matériaux de Paris Centre, FR CNRS 2482) from Sorbonne Université - Paris for Omicron XPS apparatus.

References

1 S. Bose, M. Roy and A. Bandyopadhyay, *Trends in Biotechnology*, 2012, **30**, 546–554.

2 E. Fukada and I. Yasuda, *Journal of the Physical Society of Japan*, 1957, **12**, 1158–1162.

3 R. Balint, N. J. Cassidy and S. H. Cartmell, *Tissue Engineering Part B: Reviews*, 2013, **19**, 48–57.

4 A. H. Rajabi, M. Jaffe and T. L. Arinzeh, *Acta Biomaterialia*, 2015, **24**, 12–23.

5 C. Ribeiro, V. Sencadas, D. M. Correia and S. Lanceros-Méndez, *Colloids and Surfaces B: Biointerfaces*, 2015, **136**,

Please do not adjust margins

Please do not adjust margins

46–55.
6 L. Roseti, V. Parisi, M. Petretta, C. Cavallo, G. Desando, I. Bartolotti and B. Grigolo, *Materials Science and Engineering: C*, 2017, **78**, 1246–1262.
7 A. Baji, Y. W. Mai, Q. Li and Y. Liu, *Nanoscale*, 2011, **3**, 3068–3071.
8 M. Kitsara, O. Agbulut, D. Kontziampasis, Y. Chen and P. Menasché, *Acta Biomaterialia*, 2017, **48**, 20–40.
9 F. Cristofaro, M. Gigli, N. Bloise, H. Chen, G. Bruni, A. Munari, L. Moroni, N. Lotti and L. Visai, *Nanoscale*, 2018, **10**, 8689–8703.
10 D. Lentz, A. Bach, J. Buschmann, P. Luger and M. Messerschmidt, *Chemistry - A European Journal*, 2004, **10**, 5059–5066.
11 P. Martins, A. C. Lopes and S. Lanceros-Mendez, *Progress in Polymer Science*, 2014, **39**, 683–706.
12 J. Zheng, A. He, J. Li and C. C. Han, *Macromolecular Rapid Communications*, 2007, **28**, 2159–2162.
13 F. Liu, N. A. Hashim, Y. Liu, M. R. M. Abed and K. Li, *Journal of Membrane Science*, 2011, **375**, 1–27.
14 D. Klee, Z. Ademovic, A. Bosserhoff, H. Hoecker, G. Maziolis and H. J. Erli, *Biomaterials*, 2003, **24**, 3663–3670.
15 D. Kontziampasis and M. Kitsara, *Encyclopedia of Plasma Technology*, 2016, 1097–1107.
16 A. Nandakumar, Z. Tahmasebi Birgani, D. Santos, A. Mentink, N. Auffermann, K. van der Werf, M. Bennink, L. Moroni, C. van Blitterswijk and P. Habibovic, *Biofabrication*, 2012, **5**, 015006.
17 N. Vandencasteele, D. Merche and F. Reniers, *Surface and Interface Analysis*, 2006, **38**, 526–530.
18 C. Vasile, M. C. Baican, C. M. Tibirna, C. Tuchilus, D. Debarnot, E. Pâslaru and F. Poncin-Epaillard, *Journal of Physics D: Applied Physics*, 2011, **44**, 475303.
19 K. Bazaka, O. Baranov, U. Cvelbar, B. Podgornik, Y. Wang, S. Huang, L. Xu, J. W. M. Lim, I. Levchenko and S. Xu, *Nanoscale*, 2018, **10**, 17494–17511.
20 S. B. Rodan, Y. Imai, M. A. Thiede, G. Wesolowski, D. Thompson, Z. Bar-Shavit, S. Shull, K. Mann and G. A. Rodan, *Cancer Research*, 1987, **47**, 4961 LP-4966.
21 J. Chang, M. Dommer, C. Chang and L. Lin, *Nano Energy*, 2012, **1**, 356–371.
22 H. Shao, J. Fang, H. Wang and T. Lin, *RSC Adv.*, 2015, **5**, 14345–14350.
23 R. Gregorio Jr. and E. M. Ueno, *J. Mater. Sci.*, 1999, **34**, 4489–4500.
24 X. Zhao, H. Xuan and C. He, *RSC Advances*, 2015, **5**, 81115–81122.
25 G. Beamson and D. Briggs, Eds., *The XPS of Polymers Database*, Wiley, New York, 2000.
26 I. Y. Abdullah, M. Yahaya, M. H. H. Jumali and H. M. Shanshool, 2014, **147**, 147–151.
27 S. M. Damaraju, S. Wu, M. Jaffe and T. L. Arinzeh, *Biomedical materials (Bristol, England)*, 2013, **8**, 045007.
28 P. M. Martins, S. Ribeiro, C. Ribeiro, V. Sencadas, A. C. Gomes, F. M. Gama and S. Lanceros-Méndez, *RSC Advances*, 2013, **3**, 17938.
29 M. Hoop, X. Z. Chen, A. Ferrari, F. Mushtaq, G. Ghazaryan, T. Tervoort, D. Poulikakos, B. Nelson and S. Pané, *Scientific Reports*, 2017, **7**, 1–8.
30 L. Saldaña, F. Bensiamar, A. Boré and N. Vilaboa, *Acta Biomaterialia*, 2011, **7**, 4210–4221.
31 B. M. Baker, B. Trappmann, W. Y. Wang, M. S. Sakar, I. L. Kim, V. B. Shenoy, J. A. Burdick and C. S. Chen, *Nature Materials*, 2015, **14**, 1262–1268.
32 J. Wei, T. Igarashi, N. Okumori, T. Igarashi, T. Maetani, B. Liu and M. Yoshinari, *Biomedical Materials*, , DOI:10.1088/1748-6041/4/4/045002.
33 E. Pellicer, S. Gonzalez, A. Blanquer, S. Surinach, M. D. Baro, L. Barrios, E. Ibanez, C. Nogues and J. Sort, *Journal of Biomedical Materials Research - Part A*, 2013, **101 A**, 502–517.
34 A. K, *Biomaterials*, 2000, **21**, 667–81.
35 M. Navarro, A. Michiardi, O. Castano and J. . Planell, *Journal of The Royal Society Interface*, 2008, **5**, 1137–1158.
36 M. J. Berridge, P. Lipp and M. D. Bootman, *Nature reviews. Molecular Cell Biology*, 2000, **1**, 11–21.
37 F. Hu, L. Pan, K. Zhang, F. Xing, X. Wang, I. Lee, X. Zhang and J. Xu, *PLoS ONE*, , DOI:10.1371/journal.pone.0107217.
38 W. a Catterall, *Annual Review of Cell and Developmental Biology*, 2000, **16**, 521–555.
39 R. M. Davidson, D. W. Tatakis and A. L. Auerbach, *Pflügers Archiv European Journal of Physiology*, 1990, **416**, 646–651.
40 M. Pangalos, W. Bintig, B. Schlingmann, F. Feyerabend, F. Witte, D. Begandt, A. Heisterkamp and A. Ngezahayo, *Journal of Bioenergetics and Biomembranes*, 2011, **43**, 311–322.
41 L. Khatib, D. E. Golan and M. Cho, *The FASEB Journal*, 2004, **18**, 1903–1905.
42 N. Özkucur, T. K. Monsees, S. Perike, H. Q. Do and R. H. W. Funk, *PLoS ONE*, 2009, **4**, e6131.
43 A. Marino, S. Arai, Y. Hou, E. Sinibaldi, M. Pellegrino, Y.-T. Chang, B. Mazzolai, V. Mattoli, M. Suzuki and G. Ciofani, *ACS Nano*, 2015, **9**, 7678–7689.
44 B. Ladoux and A. Nicolas, *Reports on Progress in Physics*, , DOI:10.1088/0034-4885/75/11/116601.
45 A. Ganz, M. Lambert, A. Saez, P. Silberzan, A. Buguin, R. M. Mège and B. Ladoux, *Biology of the Cell*, 2006, **98**, 721–730.
46 G. Weder, J. Vörös, M. Giazzon, N. Matthey, H. Heinzelmann and M. Liley, *Biointerphases*, 2009, **4**, 27–34.
47 G. Murillo, A. Blanquer, C. Vargas-Estevez, L. Barrios, E. Ibáñez, C. Nogués and J. Esteve, *Advanced Materials*, 2017, **29**, 1–7.
48 J. H. Scofield, *Journal of Electron Spectroscopy and Related Phenomena*, 1976, **8**, 129–137.

 This journal is © The Royal Society of Chemistry 20xx

Please do not adjust margins